nature communications

Article

https://doi.org/10.1038/s41467-025-64677-4

Full-color programmable high temperature afterglow polymers based on single-molecule emitters

Received: 18 June 2025

Accepted: 24 September 2025

Published online: 03 November 2025

Check for updates

Zhuoran Xu[1,2], Yufeng Huang[1,2], Siyu Sun[1] ✉, Liangwei Ma[1], Bingbing Ding[1], He Tian[1] & Xiang Ma[1] ✉

High-temperature afterglow organic amorphous materials expand the operational temperature beyond traditional room-temperature phosphorescent materials, broadening their potential applications. However, achieving tunable high-temperature afterglow from a single luminescent molecule remains a formidable challenge. Here, we employ host-guest anchoring coupled with single-bond rotors to achieve effective phosphorescence and tunable afterglow at high temperature simultaneously. The material demonstrates a wavelength-tunable afterglow: during heating (298 K to 473 K), the chromaticity coordinate shifts from (0.24, 0.47) to (0.18, 0.20) and the lifetime from 836 ms to 6.34 ms. The theoretical investigations reveal that the excited-state conformation of phosphors undergoes a temperature-dependent transformation, inducing the wavelength-tunable high-temperature afterglow phenomenon. This work offers a strategy for designing tunable high-temperature afterglow-emitting amorphous polymers, advancing the development of organic phosphorescent materials capable of delivering tunable high-temperature afterglow emissions.

Organic phosphorescent materials are a transformative class of luminescent materials with long lifetimes, large Stokes shifts, and stimuli-responsive characteristics, showing potential in applications such as anti-counterfeiting, bioimaging, data encryption, and sensing[1–4]. Phosphorescence originates from the radiative, spin-forbidden T_1-S_0 transition, which has inherently slow kinetics and is highly susceptible to non-radiative decay[5,6] (e.g., molecular vibrations) and oxygen quenching[7–11]. Efficient phosphorescence thus requires rigid molecular structures or environments to suppress non-radiative decay[12–22]. However, current research primarily focuses on room-temperature phosphorescence (RTP) and 77 K. This is because restricted mobility in rigid systems fails to sufficiently suppress molecular thermal agitation at elevated temperatures, facilitating non-radiative transitions and quenching RTP. This constrains the development and application of organic phosphorescent materials at high temperatures.

The development of high-temperature phosphorescent materials has attracted interests of researchers, and researchers have made significant progress in this field[19,22–30]. By employing a deep eutectic solvent strategy to restrict thermal motion[12], a fluidic high-temperature phosphorescent material capable of operating at 358 K has been proposed. The molecular planarization strategy[13] was used to suppress luminescent molecular vibrations to construct high-temperature afterglow (HTA) materials. Recently, ultra-long HTA was achieved in a boric acid system using a charge separation and recombination strategy[14]. Despite these advancements enriching HTA materials, the tunability of HTA wavelength has not yet been focused. Developing flexible and tunable HTA materials based on a single luminescent molecule remains a challenge.

Kasha's rule restricts single-molecule multicolor phosphorescence by limiting emission to the lowest excited state. To address this

[1]Key Laboratory for Advanced Materials and Feringa Nobel Prize Scientist Joint Research Center, Frontiers Science Center for Materiobiology and Dynamic Chemistry, School of Chemistry and Molecular Engineering, East China University of Science and Technology, Shanghai, PR China. [2]These authors contributed equally: Zhuoran Xu, Yufeng Huang. ✉e-mail: sunsiyu95@163.com; maxiang@ecust.edu.cn

challenge, we propose an approach that leverages a host-guest anchoring coupled with single-bond rotors to create flexible and tunable HTA materials (Fig. 1a). Hydrogen bond networks have been identified as a promising strategy for creating rigid environments that stabilize phosphorescent molecules (as guests), thereby reducing non-radiative decay rates and enhancing phosphorescence efficiency[31–43]. Dispersing rotor-containing guest molecules in hydrogen-bond-rich matrices (Polyacrylamide, PAM) restricts thermal motion through hydrogen-bond anchoring. This enables temperature-modulated multicolor phosphorescence via rotor rotation of guest molecules (Fig. 1b). Triphenylamine derivatives with good phosphorescence properties were selected here to fabricate flexible afterglow materials[44–49]. To amplify the host-guest synergy, TPCA-4 and its alkaline derivative TPCS-4 have been employed as the guest molecules (Fig. 1a). Their multiple hydrogen-bonding sites endowed the systems with good phosphorescence thermal tolerance, extending the operational temperature range beyond conventional RTP systems. These materials exhibit good photophysical properties and thermal tolerance[13,20,21,35,49–61] (Fig. 1d). Impressively, these materials exhibit pronounced afterglow under ambient daylight, with emission wavelengths dynamically shifting from 508 nm to 450 nm upon heating (Fig. 1c). This work represents advancements of tunable, flexible HTA materials using a single phosphorescent molecule, offering avenues for the design of high-performance luminescent systems under high-temperature and high-humidity conditions.

Results

Characterization of RTP Phenomena

Upon with their absorption band (365 nm, Figure. S2), the TPCA-4/TPCS-4@PAM samples fabricated by dispersing 1 wt% TPCA-4/TPCS-4 into a PAM film exhibited efficient photoluminescence (Figs. S3–6, absolute PLQY ≈ 61.7/51.7%) at room temperature, along with an impressive green afterglow persisting for over 13 s after removing UV irradiation (Figs. S7, 8 and Movie S1). Notably, their high QY (Φ_{Phos} ≈ 32.36/33.77%) enabled daylight-activated afterglow via trace UV components (Figure. S9 and Movie S2). Figs. S10, 11 show 508 nm delayed emission (lifetime ≈ 774–780 ms), consistent with their 77 K solution (Figs. S12, 13) and the RTP phenomenon. Optical microscopy revealed better dispersion homogeneity of water-soluble TPCS-4 in the PAM compared to TPCA-4 (Figs. S14, 15), leading to TPCS-4@PAM becoming the focus of subsequent studies.

Characterization of HTA Phenomena

Delayed emission spectra and lifetime measurements of TPCS-4@PAM under air and vacuum (Figs. S16–18) showed phosphorescence lifetime extended by ~100 ms in vacuum, demonstrating oxygen-dependent phosphorescence quenching. Temperature-dependent delayed emission spectra (Figs. S19, 20) and lifetime data (Figs. S21, 22) in air or vacuum confirm the phosphorescent nature of the observed afterglow and support the 5 s afterglow at 423 K (Figs. S23, 24) for TPCS-4@PAM. This phosphorescence thermal tolerance surpasses the most reported flexible organic phosphorescent materials under similar conditions. As the temperature increased, a green-to-blue afterglow transition could be observed (Figure. S23), with the details in Fig. 2a illustrating the relationship between emission wavelength, intensity, and temperature. Compared with conventional RTP materials, the TPCS-4@PAM film exhibits stronger emission intensity under elevated temperatures, which could be attributed to its drastically shortened lifetimes (from 779.58 ms to 19.03 ms) (Fig. 2d, e, detailed in Table S1). This process is further elucidated in Fig. 2b and Fig. 2c: the emission maximum blue-shifts continuously from 508 nm to 450 nm (Figs. S25, 26), accompanied by a chromaticity coordinate transition from the (0.24, 0.47) to the (0.18, 0.20). Fluorescence remained at 425 nm (Figure. S27), confirming the 450 nm delayed emission originates from phosphorescence, not thermally activated delayed fluorescence (TADF). Delayed emission spectra at 448 K under air and vacuum further reveal $^3O_2$

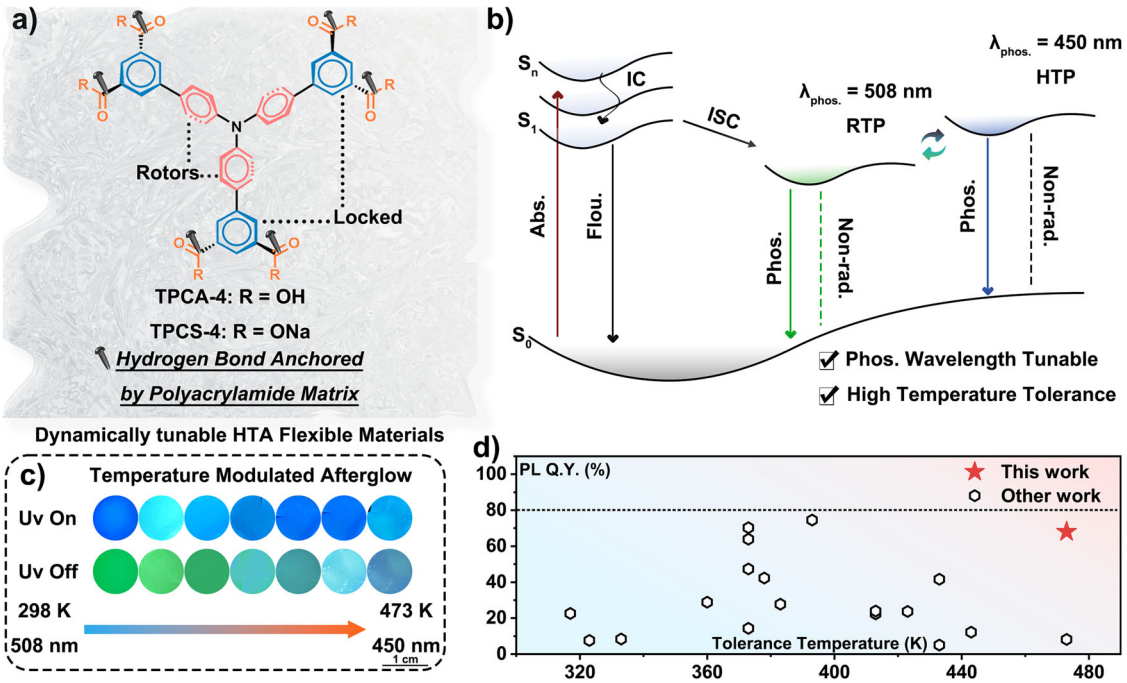

Fig. 1 | Schematic of programmable high temperature afterglow polymers. **a** Structure of the single-bond rotors and the hydrogen H-bond anchoring strategy. **b** Simplified Jablonski diagram and **c** photo of dynamic HTA. **d** Phosphorescence thermal tolerance of flexible phosphorescent materials. RTP room-temperature phosphorescence, HTA high-temperature afterglow, HTP high-temperature phosphorescence, Abs. Absorption, Flou. Fluorescence, IC internal conversion, ISC intersystem crossing, Phos. phosphorescence, Non-rad. Non-radiative Decay, PL Q.Y. photoluminescence quantum yield, K Kelvin, nm nanometer, UV ultraviolet, S_0 singlet ground state, S_n singlet excited state).

https://doi.org/10.1038/s41467-025-64677-4

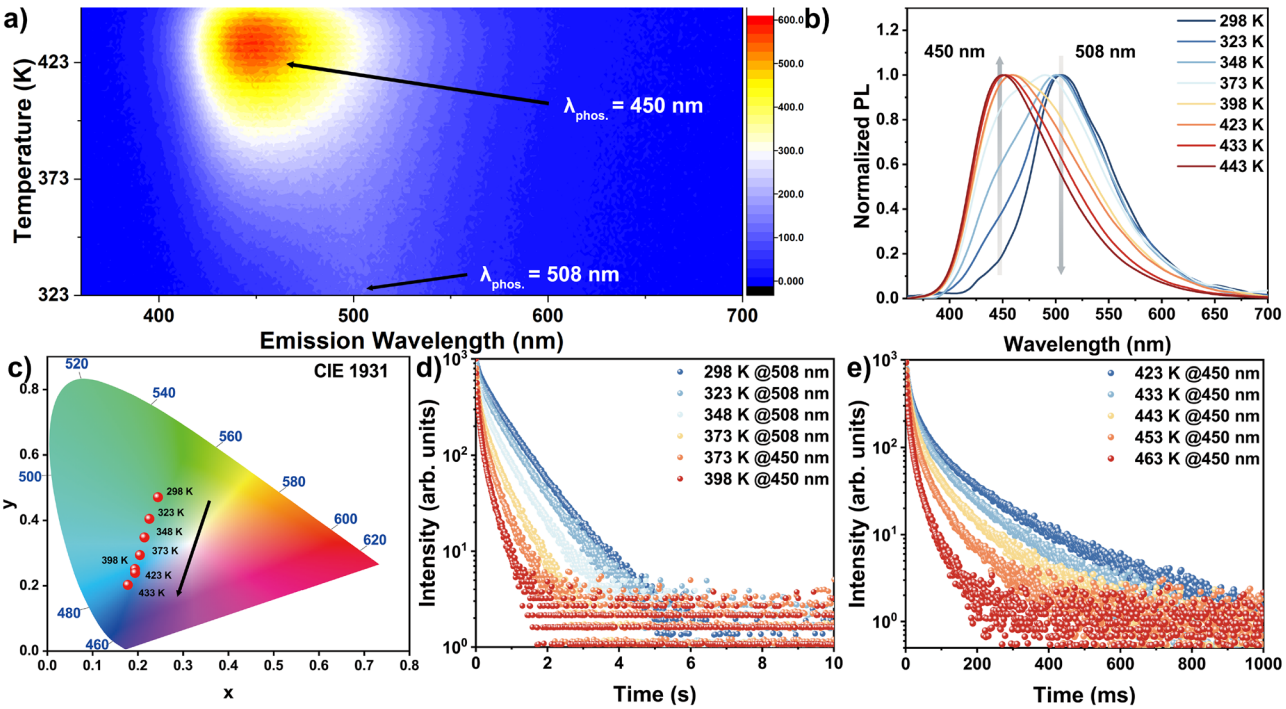

Fig. 2 | Characteristics of HTA Phenomena. a Temperature-dependent delayed emission spectra, **b** normalized delayed emission spectra, **c** CIE coordinates, and **d**, **e** lifetime spectra of TPCS-4@PAM film (Conc = 1% wt). (PL photoluminescence, CIE Commission Internationale de l'Éclairage; Conc. concentration, wt weight percent).

sensitivity (Figs. S28). The observed lifetime far exceeds the typical microsecond-to-millisecond range of TADF, aligning with phosphorescence (Figs. S29). Lifetime attenuation indicates complete quenching above 473 K, reaching the thermal tolerance limit. TPCA-4@PAM exhibits similar dynamic HTA to TPCS-4@PAM (Figs. S30, S31), with photophysical data in Table S2.

To determine the optimal guest concentration, flexible phosphorescent films with guest concentrations ranging from 0.1 wt% to 0.0001 wt% were fabricated. Powder XRD (Figure. S32) revealed that all TPCS-4@PAM films were amorphous without crystalline features. FT-IR spectroscopy (Figure. S33) confirmed that guest concentration had no significant impact in the PAM matrix across concentrations. Using the optimal excitation wavelength (Figs. S34–57, Table S3), temperature-dependent delayed emission spectra (Figs. S58–61) and lifetime measurements (Figs. S62–65, Tables S4–S7) revealed optimal properties and HTA tolerance at 0.1 wt% concentration. The lifetime retained 60 ms at 448 K (Figure. S66) with the highest PLQY at 298 K (Figs. S67–72; PLQY ≈ 67.2%, Φ_{Phos} ≈ 36.63%, Table S8). Control experiments on guest-free PAM (Figure. S73) demonstrated that the dynamic HTA properties originate from the guest molecule.

The Origins of HTA Phenomena

To investigate the origins of the HTA phenomena in these systems, guest molecules were dispersed into hydrogen-bonded polymeric matrices (PVA, PAM) and weakened non-hydrogen-bonded matrices (PDAMA, PMMA, PVB). Delayed emission spectra showed a 508 nm emission in hydrogen-bond-rich matrices (Figs. S74, 75), whereas emission was nearly quenched in weakened/non-hydrogen-bonded matrices (Figs. S76–78). Photoluminescence spectra and PLQY confirmed this: PLQY decreased from 67.1% (PAM) to 9.4% (PVB), and Φ_{Phos} from 36.63% to 5.27% (Figs. S79–86). These results demonstrate that the robust hydrogen-bonding interactions between guest and matrix molecules determine the generation and stabilization of ultralong RTP.

The hydrogen-bond interactions between guest molecules and the matrix not only determine phosphorescence properties but complement the rigid polymeric environment. Figure. S87 shows TPCS-4 structural analogs studied to clarify these effects: TPCS-1, TPCS-2, and TPCS-3 share a similar three-branched structure, each featuring one, two, and three single-bond rotors, respectively. TPCS-1 maintained emission at 443 K (Figure. S88), whereas TPCS-2 (Fig. S89, $Temperature_{max}$ = 373 K) and TPCS-3 (Figure. S90, $Temperature_{max}$ = 363 K) showed quenching with increasing rotor counts. In addition, lifetime data show analogous trends across Figs. S91–S96 (detailed in Tables S10–12). TPCS-2, and TPCS-4 exhibit the same three-branched structure, each featuring two single-bond rotors. However, TPCS-4 possesses twice the number of hydrogen-bonding functional groups compared to TPCS-2. TPCS-4 ($Temperature_{max}$ = 473 K) show better high temperature phosphorescent tolerance than TPCS-2. These results reveal that the number of single-bond rotors and hydrogen bonds jointly determines the performance of HTA.

DFT calculations (M06-2X/def2SVP) were used to investigate the wavelength-tunable HTA mechanism. 3D delayed emission spectra revealed that these flexible organic phosphorescent materials exhibit no delay time or excitation wavelength dependence at any temperature (Figs. S97–99), indicating no ground-state species variation. The dynamic afterglow behavior originates from excited-state species alterations in the T_1 state. Time-resolved emission spectra confirmed stable emission peaks at 77 K and 323 K over time, indicating a consistent triplet state. However, at 423 K, a blue shift occurs with increasing delay time, reflecting a transition from lower to higher energy states (Figure. S100). The biphenyl rotors in guest molecules generate multiple T_1-state conformations, driving temperature-dependent afterglow emission. Potential energy surface scans (Fig. 3a, b) revealed multiple T_1 energy minima versus a single minimum in S_0 and S_1 (Figure. S101), consistent with prior TRES and 3D delayed emission spectral analyses. Conformation optimization of these scan results yielded three distinct T_1 conformations and their energies (I_1^*, I_2^*, I_3^*; Fig. 3c). I_1^* and I_2^* exhibit comparable energies with a low interconversion barrier (0.677 eV, while I_3^* is thermodynamically stable but requires overcoming a high barrier (5.645 eV). Therefore, I_1^* and I_2^* are proposed to be the two potential conformations involved in

https://doi.org/10.1038/s41467-025-64677-4

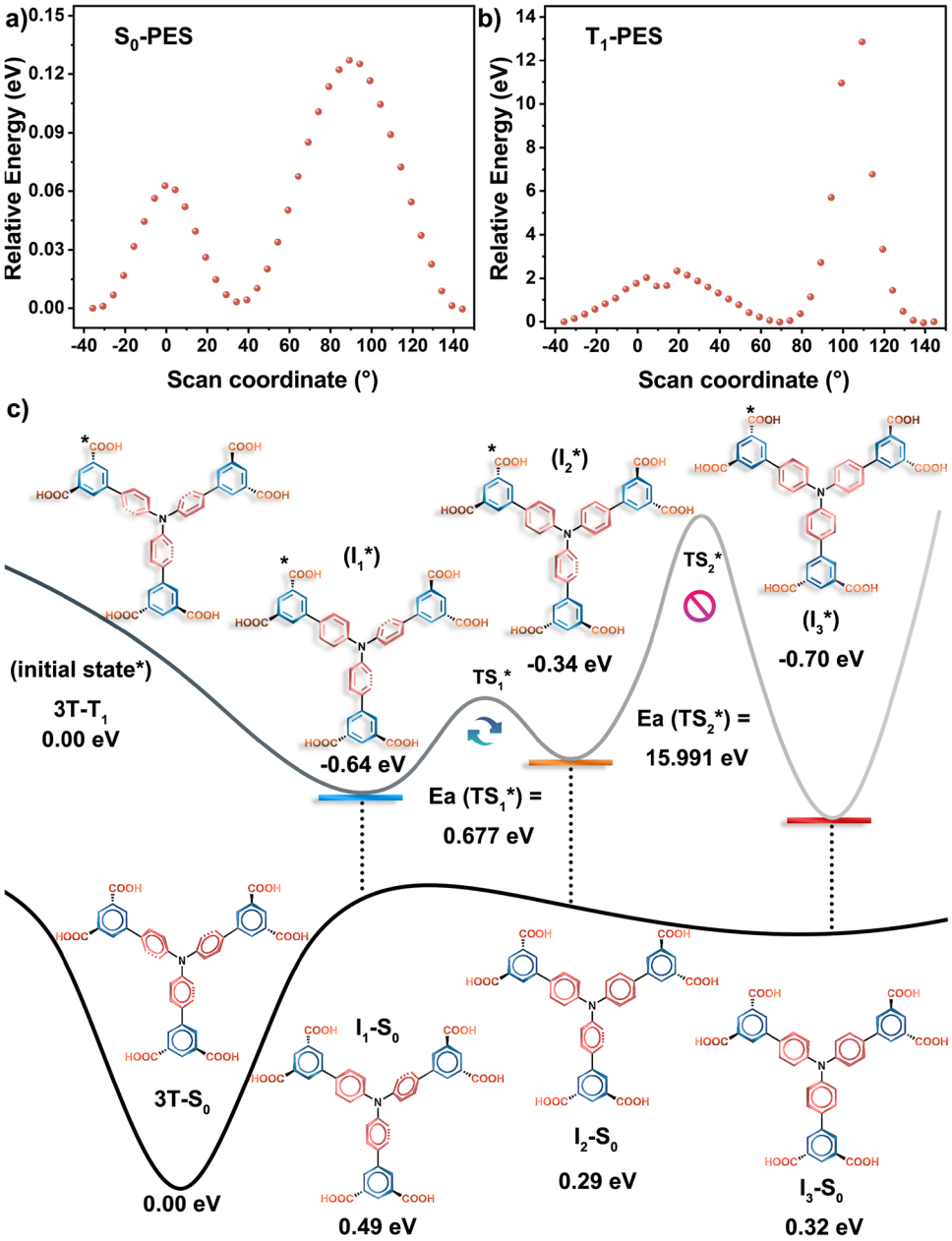

Fig. 3 | Theoretical calculations. a, **b** Potential energy surface scans for the S_0 and T_1 states of TPCA-4, and (**c**) schematic illustration of TPCA-4 with different conformations (T: twisted) calculated using M06-2X/def2SVP. (T_1 first triplet excited state, PES potential energy surface, ^{3}T-T_1 triplet twisted T_1 state, I intermediate).

the dynamic afterglow process. TD-DFT calculations (Fig. S102) revealed that the I_1^* to I_2^* conformational transition corresponds to a phosphorescence shift from 508 nm to 422 nm, consistent with experimental data.

Construction and Application of Full-Color Afterglow

The TPCS-4@PAM showed temperature-modulated dynamic afterglow with CIE coordinates changing from (0.24, 0.47) to (0.18, 0.20). Based on this, we implemented temperature-sensitive radiative energy transfer (ET) to achieve full-color afterglow. Rhodamine B (RhB) was selected as the acceptor due to its excitation spectrum overlapping with the green afterglow emission of TPCS-4@PAM (Fig. S103). By modulating the mass ratio between donor and acceptor components, full-color afterglow emission encompassing white light (CIE: 0.33, 0.37), with chromaticity coordinates shifting from (0.24, 0.47) to (0.54, 0.39) (Figs. S104, 105) was observed. At an optimal ratio, this strategy regulated delayed emission (Fig. S106) and lifetimes (Figs. S107, 108, Table S13) with ET efficiency reaching 88.66% (Fig. S109). Temperature-tunable donor molecules enabled temperature-dependent full-color afterglow systems (Fig. S110).

We developed a stimuli-responsive anti-counterfeiting ink using aqueous TPCS-4@PAM, leveraging its thermally stable and humidity-dependent afterglow properties. This ink enables programmable phosphorescence switching under UV, heat, or humidity (Fig. 4a). Besides, it can facilitate high-resolution multi-dimensional codes for real-time humidity monitoring through reversible green afterglow modulation (Fig. 4b). The hygroscopic PAM matrix governs humidity sensitivity, with adsorbed H_2O quenching emission, reversed by dehydration at 373 K, demonstrating cyclic stability over 10 heating cycles (Figs. S111–113). TPCS-4@PAM exhibited impressive stability and application potential: it maintained stable peak profiles and phosphorescent intensity during 1000 delayed emission spectral scans (Figs. S114, 115), confirming good photostability; its HTA properties persisted after 12 months under ambient conditions (Figs. S116).

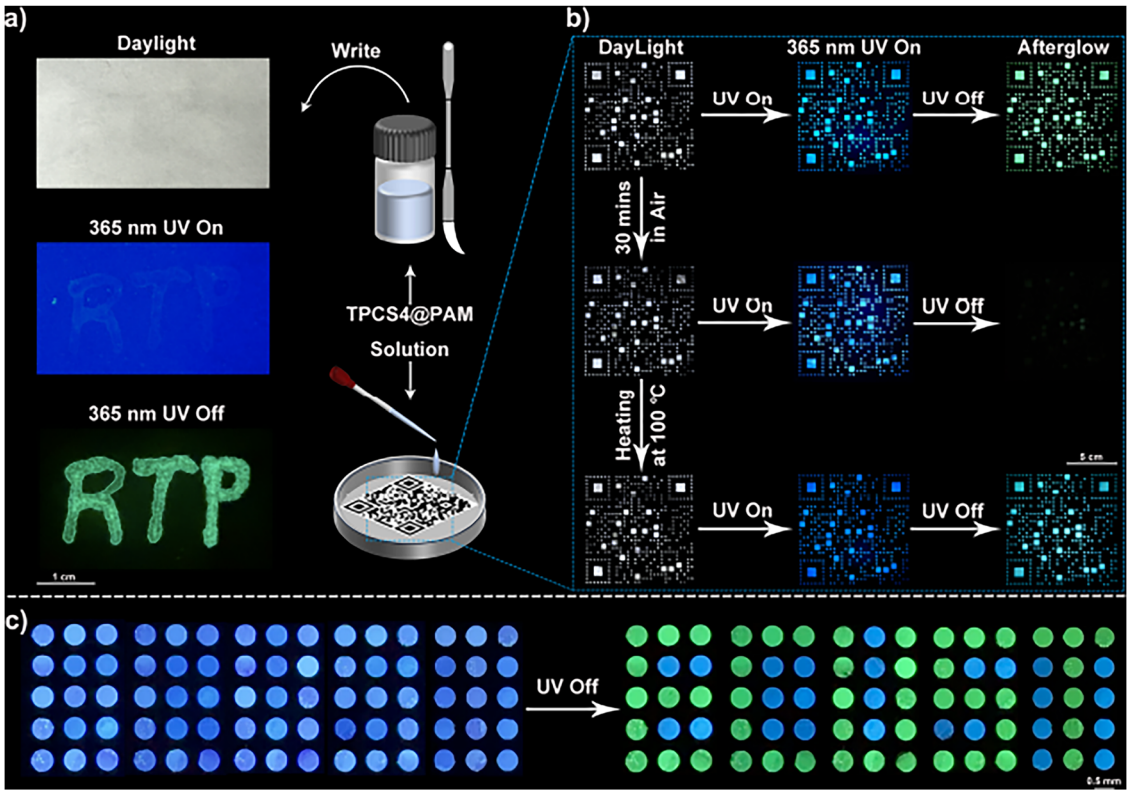

Fig. 4 | Applications of organic HTA materials for anti-counterfeiting and data encryption. a Demonstration of cryptographic anti-counterfeiting ink using TPCS-4@PAM solution. **b** Development of high-resolution multi-dimensional codes with tunable afterglow properties. **c** Creation of an ultra-long delayed emission information encryption matrix based on TPCS-1@PAM (blue) and TPCS-4@PAM (green).

Spatially resolved encryption matrices fabricated from TPCS-1@PAM and TPCS-4@PAM advance dynamic information security systems (Fig. 4c).

A simulated server room validated the high-temperature monitoring capabilities of the materials using dual-emission thermo-responsive markers (Fig. 5a). The system provides three distinct optical outputs through programmable afterglow quenching: complete emission at safe temperatures, selective blue component quenching at warning thresholds (>80°C), and full quenching in error conditions (>150 °C), with humidity-responsive behavior (Fig. 5b). Real-time monitoring demonstrated ability of HTA materials to visually map thermal profiles under operational extremes (Fig. 5c), confirming their dual-parameter (temperature/humidity) sensing utility in confined electronic environments.

Discussion

This study introduces a valuable approach to achieve daylight-excited efficient and stable phosphorescence in flexible polymer films through host-guest hydrogen-bonding. The flexible films demonstrate good phosphorescence thermal tolerance, maintaining afterglow emission for approximately 5 seconds even at elevated temperatures up to 423 K. By integrating single-bond rotors into phosphorescent cores with multiple hydrogen-bonding sites, the flexible film with rare temperature-modulated HTA property (wavelength from 508 to 450 nm; lifetime from 836 ms-298 K to 6.34 ms-473 K) has been established. Control experiments and DFT calculations establish that guest molecular conformation-modulation drive the observed phenomena. The reversible HTA ensure the erasability of the phosphorescence, highlighting the dynamic nature of these materials. These materials show potential application value in dynamic anti-counterfeiting, information encryption, and environmental temperature monitoring.

Methods

Materials

All reagents and solvents employed were commercially available and used as received without further purification. 4,4′,4″-Nitrilotribenzoic acid (TPCA-1), 4′,4‴,4⁗-Nitrilotris(([1,1′-biphenyl]-4-carboxylic acid)) (TPCA-2), 4″,4⁗,4⁗′-Nitrilotris(([1,1′:4′,1″-terphenyl]-4-carboxylic acid)) (TPCA-3) and 4,4″,4‴-Nitrilotris(([1,1′-biphenyl]-3,5-dicarboxylic acid)) (TPCA-4) was purchased from Bide Pharmatech commercially. Sodium hydroxide (NaOH) and polyacrylamide (PAM) was purchased from Adamas commercially. All chemicals have a purity of 99%.

General methods

The UV-Vis absorption spectra were obtained by a Shimadzu UV-2600 spectrophotometer. Phosphorescence, and lifetime of delayed emission spectra were recorded on an Agilent Cary Eclipse spectrophotometer. Phosphorescence mode; Delay time = 4 ms; Gate time = 5 ms. Absolute PL quantum yields were determined with a spectrometer C11347-11 (Hamamatsu, Japan). Powder X-ray diffraction (XRD) was performed on a D/max 2550VB/PC. FT-IR spectra were recorded on an INVENIO S + . All the tests were performed at 25 °C if no special statement.

Preparation of PAM solution

Weigh PAM 200 mg to the 20 mL Vial and add 16 mL H_2O into it, then stir the solution overnight until completely dissolved.

Preparation of TPCA-4@PAM film. TPCA-4 (2 mg, 0.00271 mmol) was dissolved in DMF (4 mL). The solution was added to the aforementioned PAM solution with stirring for 30 min. The mixed precursor solution was then cast into a polytetrafluoroethylene (PTFE) mold and heated to 60 °C under ambient pressure. Slow solvent evaporation over 12 h yielded a uniform flexible film. The obtained film was subsequently annealed in a vacuum oven at 60 °C for 12 h before characterization.

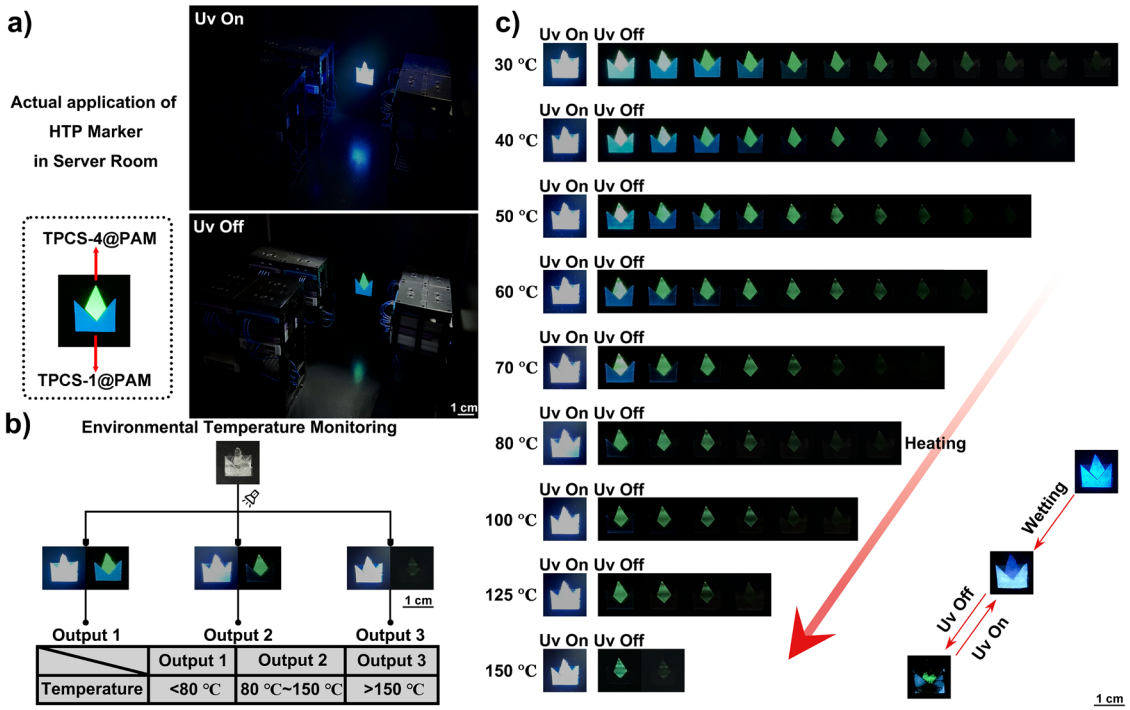

Fig. 5 | Applications of organic HTA materials for temperature monitoring. **a** Actual photographs of the server room and the temperature sensing markers. **b** Operational output signals of HTA materials across different temperature ranges within the server room. **c** Photographs of the monitoring process at various temperatures within the server room.

Preparation of TPCS-4@PAM film

After complete dissolution of the aforementioned PAM solution, TPCS-4 (2 mg, 0.0023 mmol) was added and stirred for 30 min to ensure homogeneous dissolution. The mixed precursor solution was then cast into a PTFE mold and heated to 60 °C under ambient pressure. Slow solvent evaporation over 12 h yielded a uniform flexible film. The obtained film was subsequently annealed in a vacuum oven at 60 °C for 12 h before characterization.

DFT calculation

Density functional theory (DFT) and time-dependent (TD) DFT calculations were performed with the Gaussian 09 (Revision E.01) software package. The ground-state (S_0) geometries were optimized with the M062X and def2svp basis.

Data availability

All data generated or analyzed during this study are included in this published article and its supplementary information files. All data are available from the corresponding author upon request. Source data are provided with this paper.

References

1. Ma, X.-K. & Liu, Y. Supramolecular Purely Organic Room-Temperature Phosphorescence. *Acc. Chem. Res.* **54**, 3403–3414 (2021).
2. Peng, Q., Ma, H. & Shuai, Z. Theory of Long-Lived Room-Temperature Phosphorescence in Organic Aggregates. *Acc. Chem. Res.* **54**, 940–949 (2021).
3. Shi, H. et al. Ultralong organic phosphorescence: from material design to applications. *Acc. Chem. Res.* **55**, 3445–3459 (2022).
4. Sun, S. et al. Scale effect of circularly polarized luminescent signal of matter. *Natl Sci. Rev.* **10**, nwad072 (2023).
5. Sun, S., Ma, L., Wang, J., Ma, X. & Tian, H. Red-light excited efficient metal-free near-infrared room-temperature phosphorescent films. *Natl Sci. Rev.* **9**, nwab085 (2022).
6. Sun, S., Fan, Y., Ma, L., Han, Y. & Ma, X. Local constraints on junctions to strengthen near-infrared phosphorescence of organic dyes. *J. Phys. Chem. Lett.* **12**, 11919–11925 (2021).
7. Bolton, O., Lee, K., Kim, H.-J., Lin, K. Y. & Kim, J. Activating efficient phosphorescence from purely organic materials by crystal design. *Nat. Chem.* **3**, 205–210 (2011).
8. Gu, L. et al. Colour-tunable ultra-long organic phosphorescence of a single-component molecular crystal. *Nat. Photonics* **13**, 406–411 (2019).
9. Song, J., Ma, L., Sun, S., Tian, H. & Ma, X. Reversible Multilevel Stimuli-Responsiveness and Multicolor Room-Temperature Phosphorescence Emission Based on a Single-Component System. Angew. *Chem. Int. Ed.* **61**, e202206157 (2022).
10. Song, J. et al. An elastic organic crystal with multilevel stimuli-responsive room temperature phosphorescence. *Matter* **6**, 2005–2018 (2023).
11. Xie, Y. et al. How the molecular packing affects the room temperature phosphorescence in pure organic compounds: Ingenious molecular design, detailed crystal analysis, and rational theoretical calculations. *Adv. Mater.* **29**, 1606829 (2017).
12. Sun, S., Wang, J., Ma, L., Ma, X. & Tian, H. A universal strategy for organic fluid phosphorescence materials**. *Angew. Chem. Int. Ed.* **60**, 18557–18560 (2021).
13. Chen, K. et al. Twofold rigidity activates ultralong organic high-temperature phosphorescence. *Nat. Commun.* **15**, 1269 (2024).
14. Jiang, P. et al. Thermal modulation of exciton recombination for high-temperature ultra-long afterglow. *Angew. Chem. Int. Ed.* **64**, e202421036 (2025).
15. Gu, K. et al. A gated strategy stabilizes room-temperature phosphorescence. *Aggregate* **4**, e337 (2023).
16. Liu, X. W. et al. Photo-thermo-induced room-temperature phosphorescence through solid-state molecular motion. *Nat. Commun.* **13**, 3887 (2022).

17. Liu, Y. et al. Carbon dots-inked paper with single/two-photon excited dual-mode thermochromic afterglow for advanced dynamic information encryption. *Adv. Mater.* **36**, 2403775 (2024).
18. Lou, Q. et al. Thermally Enhanced and Long Lifetime Red TADF Carbon Dots via Multi-Confinement and Phosphorescence Assisted Energy Transfer. *Adv. Mater.* **35**, 2211858 (2023).
19. Wang, H. et al. Abnormal thermally-stimulated dynamic organic phosphorescence. *Nat. Commun.* **15**, 2134 (2024).
20. Xu, L., Wei, H., Xie, G., Xu, B. & Zhao, J. Ultralong MRTADF and room-temperature phosphorescence enabled color-tunable and high-temperature dual-mode organic afterglow from indolo[3,2-b]carbazole. *Adv. Funct. Mater.* **34**, 2402428 (2024).
21. Zhang, Y., Chen, Y., Li, J., Liu, S. & Liu, Y. Mechanical stretch α-cyclodextrin pseudopolyrotaxane elastomer with reversible phosphorescence behavior. *Adv. Sci.* **11**, 2307777 (2024).
22. Ding, Y. et al. Ultrahigh-temperature long-persistent luminescence from B_2O_3-confined polycyclic aromatic compounds. *J. Am. Chem. Soc.* **146**, 25211–25220 (2024).
23. Yang, J., Fang, M. & Li, Z. Stimulus-responsive room temperature phosphorescence materials: internal mechanism, design strategy, and potential application. *Acc. Mater. Res.* **2**, 644–654 (2021).
24. Wu, M. et al. High-Temperature-Available Organic Blue Phosphorescence for Optical Waveguide. *Adv. Funct. Mater.* 2505113 https://doi.org/10.1002/adfm.202505113 (2025).
25. Wang, M. et al. Building a highly stable red/near infrared afterglow library with highly branched structures. *Adv. Mater.* **37**, 2415446 (2025).
26. Singh, M. et al. Achieving high-temperature phosphorescence by organic cocrystal engineering. *Angew. Chem. Int. Ed.* **63**, e202319694 (2024).
27. Luo, W. et al. Leveraging multivalent assembly towards high-temperature liquid-phase phosphorescence. *Angew. Chem. Int. Ed.* **64**, e202423650 (2025).
28. Liu, X., Liao, Q., Yang, J., Li, Z. & Li, Q. Unveiling one-to-one correspondence between excited triplet states and determinate interactions by temperature-controllable blue-green-yellow afterglow. *Angew. Chem. Int. Ed.* **62**, e202302792 (2023).
29. Fan, Y., Li, Q. & Li, Z. Afterglow bio-applications by utilizing triplet excited states of organic materials. *Sci. China Chem.* **66**, 2930–2940 (2023).
30. Dong, M. et al. Temperature-adaptive organic scintillators for X-ray radiography. *J. Am. Chem. Soc.* **147**, 4069–4078 (2025).
31. Guo, H. et al. Red room temperature phosphorescence from lignin. *Angew. Chem. Int. Ed.* **64**, e202421112 (2025).
32. Gao, M. et al. New molecular photoswitch based on the conformational transition of phenothiazine derivatives and corresponding triplet emission properties. *J. Am. Chem. Soc.* **147**, 2653–2663 (2025).
33. Miao, Y. et al. Stable and ultralong room-temperature phosphorescent copolymers with excellent adhesion, resistance, and toughness. *Sci. Adv.* **10**, eadk3354 (2024).
34. Ma, D.-X. et al. Nylons with highly-bright and ultralong organic room-temperature phosphorescence. *Nat. Commun.* **15**, 4402 (2024).
35. Wei, J. et al. Conformation-dependent dynamic organic phosphorescence through thermal energy driven molecular rotations. *Nat. Commun.* **14**, 627 (2023).
36. Li, D. et al. Ultralong room-temperature phosphorescence with second-level lifetime in water based on cyclodextrin supramolecular assembly. *ACS Nano* **17**, 12895–12902 (2023).
37. Gao, L. et al. Stepwise taming of triplet excitons via multiple confinements in intrinsic polymers for long-lived room-temperature phosphorescence. *Nat. Commun.* **14**, 7252 (2023).
38. Zhang, Y. et al. Cross-linked polyphosphazene nanospheres boosting long-lived organic room-temperature phosphorescence. *J. Am. Chem. Soc.* **144**, 6107–6117 (2022).
39. Qian, G. et al. Structural and chemical evolution in layered oxide cathodes of lithium-ion batteries revealed by synchrotron techniques. *Natl Sci. Rev.* **9**, nwab146 (2022).
40. Zhang, Y. et al. Large-Area, Flexible, Transparent, and Long-Lived Polymer-Based Phosphorescence Films. *J. Am. Chem. Soc.* **143**, 13675–13685 (2021).
41. Peng, H. et al. On-demand modulating afterglow color of water-soluble polymers through phosphorescence FRET for multicolor security printing. *Sci. Adv.* **8**, eabk2925 (2022).
42. Zhang, Z. et al. Modulating emission of boric acid into highly efficient and color-tunable afterglow via dehydration-induced through-space conjugation. *Adv. Sci.* **10**, 2300139 (2023).
43. Hou, H. et al. Thermal annealing effects on long-lived fluorenol room temperature phosphorescence for styrene detection. *Angew. Chem. Int. Ed.* **63**, e202411323 (2024).
44. Xiong, S. et al. Achieving tunable organic afterglow and UV-irradiation-responsive ultralong room-temperature phosphorescence from pyridine-substituted triphenylamine derivatives. *Adv. Mater.* **35**, 2301874 (2023).
45. Bai, J. et al. Conformation-controlled double phosphorescence components from a single organic molecule: time-dependent and excitation-dependent wide-range afterglow color change. *Adv. Funct. Mater.* **35**, 2411496 (2025).
46. Yang, H. et al. Efficient and ultralong room temperature phosphorescence from isolated molecules under visible light excitation. *J. Am. Chem. Soc.* **147**, 1474–1481 (2025).
47. Yan, S. et al. Highly efficient amorphous polymer-based ultralong phosphorescence enabled by intense repulsive interactions. *Adv. Funct. Mater.* **35**, 2413878 (2025).
48. Wu, S., Wang, T. & Zysman-Colman, E. Hydrogen-bonded supramolecular network triggers high-efficiency blue room-temperature phosphorescence. *CCS Chem.* **6**, 2727–2740 (2024).
49. Wu, Z. et al. Positional isomerism toward tunable organic afterglow and reversible photoactivation behavior for anti-counterfeiting and encryption. *Adv. Funct. Mater.* **35**, 2415285 (2025).
50. Tang, S. et al. Cycloolefin copolymers with a multiply rigid structure for protecting triplet exciton from thermo- and moisture-quenching. *Adv. Mater.* **37**, 2416397 (2025).
51. Chen, Y., Xu, Z., Yu, M. & Fu, H. High-temperature dynamic organic phosphorescence based on cyclodextrins supramolecular assemblies. *ACS Appl. Mater. Interfaces* **17**, 24351–24358 (2025).
52. Wang, Y. et al. Host-guest doped room/high-temperature phosphorescence of diarylfuro[3,2-b]pyridine derivatives. *Chem. Eng. J.* **489**, 150919 (2024).
53. Li, N. et al. Color-tunable room-temperature phosphorescence from non-aromatic-polymer-involved charge transfer. *Adv. Sci.* **11**, 2404698 (2024).
54. Jin, L. et al. Hierarchical dual-mode efficient tunable afterglow via J-aggregates in single-phosphor-doped polymer. *Angew. Chem. Int. Ed.* **63**, e202410974 (2024).
55. Niu, Y. et al. A universal strategy for achieving dual cross-linked networks to obtain ultralong polymeric room temperature phosphorescence. *Sci. China Chem.* **66**, 1161–1168 (2023).
56. Lv, H. et al. Highly stable metal-free long-persistent luminescent copolymer for low flicker AC-LEDs. Angew. Chem. *Int. Ed.* **61**, e202204209 (2022).
57. Zhu, Y. et al. Ultralong polymeric room temperature phosphorescence materials fabricated by multiple hydrogen bondings resistant to temperature and humidity. *Adv. Opt. Mater.* **9**, 2100782 (2021).
58. Wu, H. et al. Molecular phosphorescence in polymer matrix with reversible sensitivity. *ACS Appl. Mater. Interfaces* **12**, 20765–20774 (2020).
59. Wu, B. et al. Ultralong and high-efficiency room temperature phosphorescence of organic-phosphors-doped polymer films enhanced by 3D network. *Adv. Opt. Mater.* **8**, 2001192 (2020).

60. Qin, W. et al. Simultaneous promotion of efficiency and lifetime of organic phosphorescence for self-referenced temperature sensing. *Chem. Eng. J.* **400**, 125934 (2020).
61. Cai, S. et al. Enabling long-lived organic room temperature phosphorescence in polymers by subunit interlocking. *Nat. Commun.* **10**, 4247 (2019).

Acknowledgements

This work was supported by the National Natural Science Foundation of China (22125803, T2488302, and 22020102006 to X.M.), the Science and Technology Commission of Shanghai Municipality (grant No. 24DX1400200 to X.M.), the Postdoctoral Fellowship Program of CPSF (GZB20240220 to S.S.), the Natural Science Foundation of Shanghai (25ZR1402108 to S.S.), and the Fundamental Research Funds for the Central Universities. We thank Y.H. Sun for helpful discussions.

Author contributions

Z.X.: Conceptualization, Formal analysis, Investigation, Methodology; Visualization, Writing; Y.H.: performed the experiments; S.S.: Conceptualization, Formal analysis, Investigation, Methodology, Visualization, Writing, Funding acquisition; L.M.: Validation; B.D.: Validation; H.T.: Writing revision, Funding acquisition, Project administration, Supervision; X.M.: Writing revision, Funding acquisition, Resources, Project administration, Supervision.

Competing interests

The authors declare no competing interests.

Additional information

Supplementary information The online version contains supplementary material available at https://doi.org/10.1038/s41467-025-64677-4.

Correspondence and requests for materials should be addressed to Siyu Sun or Xiang Ma.

Peer review information *Nature Communications* thanks Swadhin Garain and the other, anonymous, reviewers for their contribution to the peer review of this work. A peer review file is available.